Plasmonic metasurface for optical rotation

Plasmonic metasurface for optical rotation

Dandan Wen,[1] Fuyong Yue,[1] Chunmei Zhang,[1] Xiaofei Zang,[1,2] Huigang Liu,[1,3] Wei Wang,[1] Xianzhong Chen[1, a)]

[1]SUPA, Institute of Photonics and Quantum Sciences, School of Engineering and Physical Sciences, Heriot-Watt University, Edinburgh, EH14 4AS, UK

[2]Shanghai Key Lab of Modern Optical System, University of Shanghai for Science and Technology, No.516 JunGong Road, Shanghai 200093, China

[3]Tianjin Key Laboratory of Optoelectronic Sensor and Sensing Network Technology, College of Electronic Information and Optical Engineering, Nankai University, Tianjin 300350, China

a) Corresponding author: x.chen@hw.ac.uk

Plasmonic metasurface for optical rotation

Abstract

Optical activity, known as optical rotation, has found many applications ranging from optical isolators and concentration determination to sophisticated organic structure analysis. Miniaturization and integration are two continuing trends in the production of photonic devices. However, there are fundamental or technical challenges to further reduce the thickness of the optical elements to generate desirable polarization rotation with broadband and high efficiency. Here in this paper, an efficient method to realize optical rotation for the visible and near infrared light is experimentally demonstrated using an ultrathin metasurface. The polarization rotation originates from the additional phase difference between the two circular polarizations induced by the rectangular metasurface phase grating. Benefiting from the advantages of the reflective metasurface, the fabricated highly efficient device can operate in the broadband. Good agreement between the designed rotation angle and measured results renders this technique very attractive for the practical application in device miniaturization and system integration.

Key words: geometric phase, metasurface, rectangular phase grating, optical rotation

Introduction

Optical rotation is the rotation of the polarization plane of a linearly polarized light beam as it travels through certain materials [1]. Since its first observation by Arago in 1811, optical rotation has been widely used in a number of places [2-4]. Conventionally, optical rotation occurs in chiral materials whose structures are distinguishable from their mirror images. The effect is generally weak in naturally occurring chiral materials (such as quartz); hence a minimum optical path length must be available in order to reach a desired rotation range, making the devices very bulky. Faraday effect proves to be a versatile mechanism to manipulate light rotation, but the Faraday effect in currently available magneto-optical materials is also very weak (e.g., typical size of a Faraday rotator is in the order of centimetres). Although the combination of plasmonics and magneto-optics can enhance the polarization rotation [5, 6], the rotation angle through optically thin material still has room for improvement.

Optical metamaterials are artificial media, whose optical properties are determined by their geometry structures instead of constituent components, which have opened avenues in the manipulation of polarization [7-10]. However, the technical challenges in fabrication and high-energy loss in 3D metamaterials have hindered their application in the visible range. Benefiting from the easy fabrication procedure and the unprecedented capability to manipulate light propagation, metasurfaces [11-15] provide an effective way for the polarization control. Limited polarization rotation angles can be achieved through chiral metasurfaces [16, 17],

which are two dimensional counterparts of conventional 3D chiral materials. Metasurface-based half waveplates [18-20] can mimic the functionality of birefringent materials, which impart phase difference of π between the two cross polarized light components to realize optical rotation. However, since the geometry of the antenna affects its response to the incident light significantly, it is important to precisely control the feature size of the designed nanostructures, or else the polarization rotation angle will be shifted from the original design. Optical rotation can also be realized through a metasurface consisting of two subunits that generate two co-propagating waves with equal amplitudes, orthogonal polarizations, and spatial separation-induced phase difference [21, 22]. Nevertheless, unwanted higher diffraction orders may be induced if the operating wavelength is less than the double distance of neighboring antennas due to the intersecting distribution of the two subunits. Although dielectric metasurfaces have been proposed to manipulate light polarization with high efficiency in the transmission mode [23, 24], it is fundamentally difficult to achieve a broadband performance since the geometry of the nano-structures are designed to operate for a given wavelength. Thus, a simple and elegant method to generate arbitrary polarization rotation within optically thin films with great fabrication tolerance and broadband performance is highly desirable for device miniaturization and system integration.

In this work, an effective method to realize optical rotation with a metasurface is proposed and experimentally verified. By using the rectangular phase grating generated by the metasurface, the designed device can decompose the incident linearly polarized light into right circularly polarized (RCP) light and left circularly polarized (LCP) light, and add a required phase difference between them, leading to the polarization rotation of the incident light [Fig. 1(a)]. The rotation angle of the reflected light is solely determined by the two-phase steps defined in the metasurface, which can reach arbitrary rotation angles from 0 to 2π. Since each phase step is based on the geometric phase whose value is solely determined by the orientation of the nanorod, the developed devices have great fabrication tolerance and broadband performance.

Materials and Methods

Geometric phase in optics originates from the coupling between intrinsic angular momentum and rotations of coordinates. The most studied manifestations of geometric phase are spin-redirection phase and Pancharatnam-Berry (P-B) phase [25]. In this paper, we will concentrate on a specific P-B phase, which is generated through the transformation of the circularly polarized (CP) light by an anisotropic nanorod [26]. Upon the illumination of CP light, part of the reflected light from the metasurface reserves the handedness of the incident light and picks up a phase of $\pm 2\varphi$. The angle φ represents the orientation angle of the nanorod and the sign '+' or '-' is determined by the handedness of the incident light. The term 'geometric phase' in this paper refers to this specific P-B phase of $\pm 2\varphi$. Since the value of the geometry phase is determined by the orientation of the nanorod, a sampled phase function can be represented by an inhomogeneous metasurface consisting of an array of nanorods with different orientations. In our design, we leverage on the recent advancement of reflective-type metasurfaces, which can work in broadband with high efficiency [26-28]. As

shown in Fig. 1(b), the metasurface is composed of a silver nanorod array on the top, a SiO_2 spacer in the middle and a silver ground layer at the bottom.

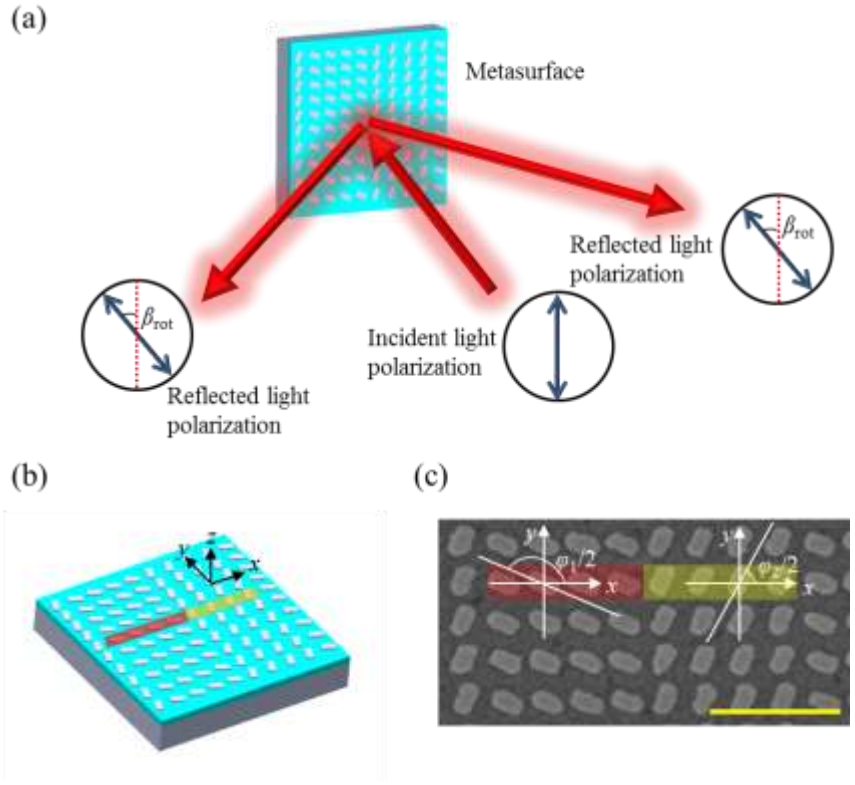

FIG. 1. (a) Schematic of the polarization rotation by a metasurface. The linearly polarized incident light impinges on the metasurface, and its polarization direction is rotated by a designed angle β_{rot}. Here β_{rot} is formed by the oscillation direction of the reflected light and the vertical direction of the reflection plane. (b) Schematic of the rectangular phase grating based on the metasurface. The metasurface consists of three layers: silver nanorods on the top, a SiO_2 spacer and a silver ground layer. Each phase step contains four nanorods (colored with red and yellow) and two phase steps form a single unit. (c) SEM image of the fabricated metasurface. The scale bar is 1 μm.

Here, the metasurface is utilized to generate a rectangular phase grating, which contains two phase steps φ_1 and φ_2 in a single period. As shown in Figs. 1(b)-(c), the nanorods in red and yellow have the orientation angles of $\varphi_1/2$ and $\varphi_2/2$, respectively. When the incident RCP light shines on the metasurface, the reflected RCP light from the red (yellow) nanorods picks up a geometric phase of $\varphi_1(\varphi_2)$. The reflected RCP light from the two subunits has equal amplitude since it is only determined by the geometry of the nanorod, not the orientation. The reflected LCP light has the equal amplitude with that of the RCP light [14]. The orientations of the nanorods change along the *x*-direction [Fig. 1(b)] and they are repeated along the *y*-direction.

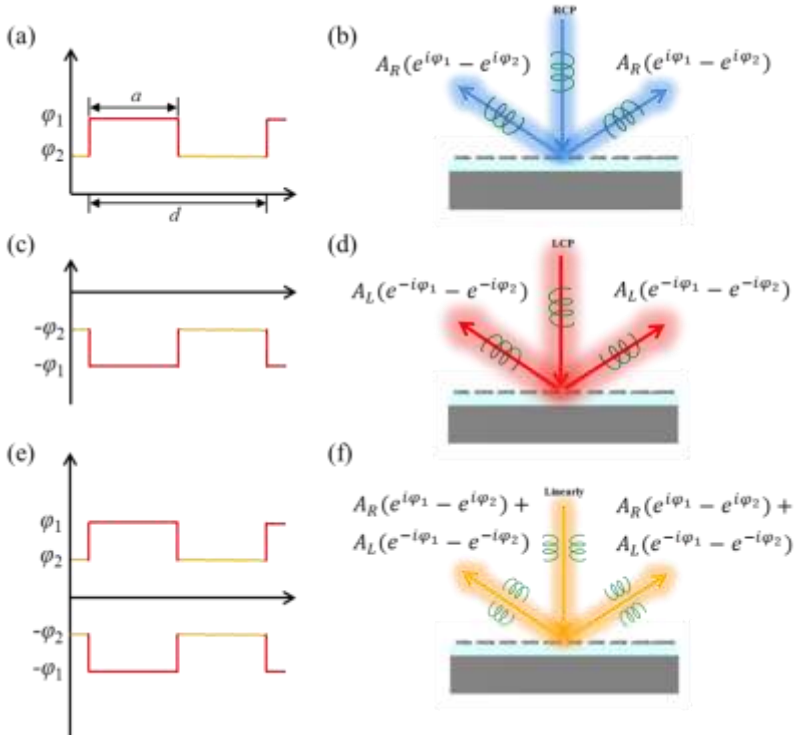

FIG. 2. Design of the metasurface for polarization rotation. (a) When the rectangular phase grating is under the illumination of RCP light, the curve shows the phase profile of reflected RCP light. (b) The ±1st orders of the reflected RCP light are located symmetrically on both sides of the incident direction with the complex amplitude $A_R\left(e^{i\varphi_1}-e^{i\varphi_2}\right)$. (c) Phase profile of the reflected LCP light from the metasurface when the incident light is LCP. (d) The reflected ±1st orders of LCP light both have the complex amplitude $A_L\left(e^{-i\varphi_1}-e^{-i\varphi_2}\right)$. (e) When the incident light is linearly polarized, the phase profiles are different for its RCP and LCP components. (f) The +1st order of RCP and LCP reflected light have the same amplitude (A_R=A_L) and propagation direction, but they have a phase difference $\Delta\Phi$. The two beams superpose and form a linearly polarized light with a rotated polarization direction. So do the -1st order of RCP and LCP reflected light.

If the rectangular phase grating is under the illumination of RCP light, the RCP reflected light will have the phase profile as shown in Fig. 2(a). The reflection coefficient for the RCP reflected light is [29, 30]

$$t(x_0,y_0)=\left(e^{i\varphi_1}-e^{i\varphi_2}\right)rect\left(\frac{x_0}{a}\right)*\frac{1}{d}comb\left(\frac{x_0}{d}\right)+e^{i\varphi_2} \tag{1}$$

The phase steps of φ_1 has the lengths of a and the period length is d. The function *rect* denotes the rectangular function and *comb* denotes the Dirac comb function. According to the Fraunhofer diffraction equation, the light diffracted by the grating in the far field at a distance z has the amplitude

$$U(x_1,y_1)=\frac{1}{i\lambda z}e^{ikz}e^{\left[i\frac{k}{2z}(x_1^2+y_1^2)\right]}T\left(f_x,f_y\right)_{f_x=\frac{x_1}{\lambda z},f_y=\frac{y_1}{\lambda z}} \tag{2}$$

Where λ and k represent the wavelength and wavenumber of the incident light, respectively. $T(f_x, f_y)$ is the Fourier transformation of $t(x_0, y_0)$ and we have its expression

$$T\left(f_x,f_y\right)=\left(e^{i\varphi_1}-e^{i\varphi_2}\right)\frac{a}{d}\mathrm{sinc}\left(\frac{ax_1}{\lambda z}\right)\sum_{n=-\infty}^{+\infty}\delta\left(\frac{x_1}{\lambda z}-\frac{n}{d},\frac{y_1}{\lambda z}\right)+e^{i\varphi_2}\delta\left(\frac{x_1}{\lambda z},\frac{y_1}{\lambda z}\right) \tag{3}$$

According to Eq.(3), the schematic of the ±1st orders RCP reflected light is shown in Fig. 2(b). Equations (1)-(3) are only valid for the RCP incident light. The phase function of the metasurface will be added to a minus sign if the incident light changes to LCP [Fig. 2(c)], and then Eq. (3) changes into

$$T'(f_x, f_y) = \left(e^{-i\varphi_1} - e^{-i\varphi_2}\right)\frac{a}{d}\,\mathrm{sinc}\left(\frac{ax_1}{\lambda z}\right)\sum_{n=-\infty}^{+\infty}\delta\left(\frac{x_1}{\lambda z} - \frac{n}{d}, \frac{y_1}{\lambda z}\right) + e^{-i\varphi_2}\delta\left(\frac{x_1}{\lambda z}, \frac{y_1}{\lambda z}\right) \quad (4)$$

The ±1st orders LCP reflected light is schematically shown in Fig. 2(d) based on Eq. (4).

For the linearly polarized incident light that contains equal RCP and LCP components, the metasurface responds differently to the two components [Fig. 2(e)]. Equations (3) and (4) show that the n^{th} (n=±1, ±2…) order reflected RCP and LCP light both propagate along the same direction, which forms an angle of arctan($\lambda n/d$) with the normal of the metasurface. Besides, the complex amplitudes of the n^{th} order RCP and LCP light beams ($U_{n\text{-}RCP}$ and $U_{n\text{-}LCP}$) have the equal amplitude since

$$\frac{|U_{n-RCP}|}{|U_{n-LCP}|} = \frac{|e^{i\varphi_1} - e^{i\varphi_2}|}{|e^{-i\varphi_1} - e^{-i\varphi_2}|} = 1 \quad (5)$$

More importantly, the rectangular phase grating induces a phase difference $\Delta\Phi$ between them

$$\Delta\Phi = phase(U_{n-RCP}) - phase(U_{n-LCP})$$

$$= phase\left(e^{i\varphi_1} - e^{i\varphi_2}\right) - phase\left(e^{-i\varphi_1} - e^{-i\varphi_2}\right) \quad (6)$$

The function *phase* is used to calculate the phase angles of the complex numbers $e^{i\varphi_1} - e^{i\varphi_2}$ and $e^{-i\varphi_1} - e^{-i\varphi_2}$. If φ_1 and φ_2 are assumed to be

$$\varphi_1 = \pi + \alpha \quad (7)$$

$$\varphi_2 = 0 + \alpha \quad (8)$$

Equation (6) changes into

$$\Delta\Phi = 2\alpha \quad (9)$$

Since the reflected RCP and LCP components have the equal amplitude, same propagation direction and a phase difference $\Delta\Phi$, the two components superpose and form a linearly polarized light with rotated polarization direction. For the *y*-polarized incident light (Fig. 1), it can be deduced that the phase difference $\Delta\Phi$ is the double of β_{rot}

$$\Delta\Phi = 2\beta_{rot} \quad (10)$$

Equations (9)-(10) show that α has the same value of the optical rotation angle β_{rot}, providing an elegant way to design a metasurface for optical rotation. For the desired optical rotation angle β_{rot}, the values of { φ_1, φ_2} are {β_{rot}+π, β_{rot}}, which are then encoded onto the metasurface as show in Fig. 1(b).

Results and Discussion

To verify polarization rotation method proposed above, four samples are designed to rotate the 90°-polarized (*y*-polarized as shown in in Fig. 1) incident light by the angles of β_{rot}=45°, 90°, 135° and 180°, respectively. In other words, the polarization directions (the angle between the oscillation directions of the light and the *x*-direction as shown in Fig. 1) of the reflected light from samples 1-4 are designed be -45°, 0°, 45° and 90°, respectively. Based on the discussion in last section, the values of {φ_1, φ_2} should be {225°, 45°} for sample 1, {270°, 90°} for sample 2, {315°, 135°} for sample 3 and {360°, 180°} for sample 4. We take sample 3 for an example and its SEM image is shown in Fig. 1(c).

All the samples have nanorods of the same geometry, which is 75 nm wide, 200 nm long and 30 nm high. A titanium adhesive layer of 3 nm is added between the silver nanorods and the SiO_2 spacer. The distance between the neighboring nanorods is 300 nm along the horizontal and vertical directions. Each metasurface contains 1000×1000 nanorods that yields a total size of 300 μm×300 μm.

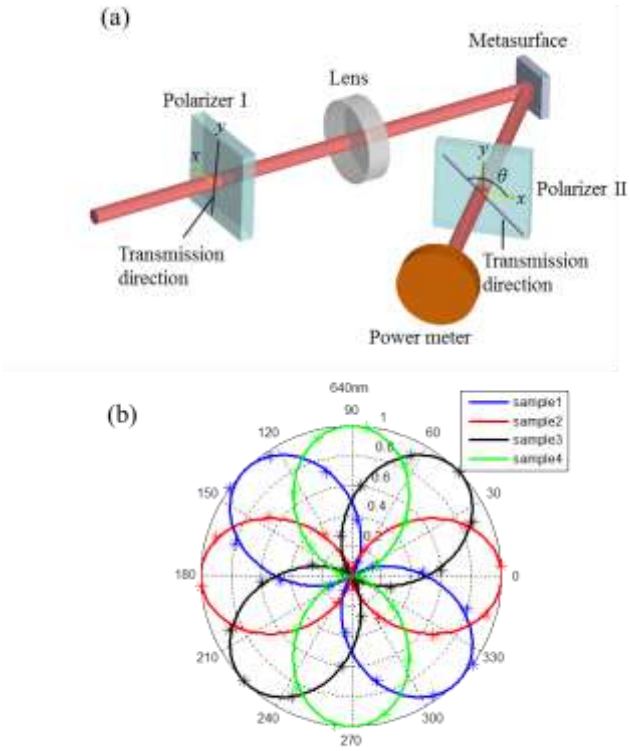

FIG. 3. Experimental setup and polarization measurement. (a) Schematic of the experimental setup. After passing through polarizer I with the transmission direction along the *y*-axis, the light is weakly focused by a lens and incident onto the metasurface at normal incidence. The power of the +1th order reflected light is recorded by the power meter after passing through polarizer II with various rotation angles θ. (b) The four solid curves represent the simulated results for the ideal linear polarization states with designed polarization directions of -45° 0°, 45° and 90°, respectively. The discrete asterisks with blue, red, black and green colors represent the measurements for samples 1, 2, 3, and 4, respectively. The experimental results are obtained at the wavelength of 640 nm. The experimental results are normalized here. Although the four samples are fabricated under the same process, their reflection peaks are slightly different due to the fabrication nonuniformity.

The schematic of the measurement system is shown in Fig. 3(a). The incident light from the supercontinuum laser (NKT, SuperK Extreme) passes through polarizer I with its transmission axis along the *y* axis. Then the *y*-polarized light is weakly focused by a plano-convex spherical lens (*f*=75mm) to make sure that energy of the incident light is concentrated on the metasurface. Although the focusing process will tilt the incident light, the tilt angle is very small and can be ignored. The sample under test is mounted on a 2D translation stage, allowing for position adjustment in the plane perpendicular to the incident direction. The $+1^{st}$ order reflected light is analyzed by rotating polarizer II with different angles θ and the power is recorded by a power meter. It should be noted that the metasurface is originally designed to work under the plane wave illumination. The lightly focused incident light has a diameter much larger than that of the metasurface; then the spatial phase nonuniformity of the incident light is very subtle over the metasurface scale.

The simulated curve of $I(\theta)$ for the reflected light with ideal -45°-polarization is shown in Fig. 3(b) (blue color). Similarly, the red, black and green curves represent the simulated results of $I(\theta)$ for the linear polarization of 0°, 45° and 90°, respectively. The position of the curve peak denotes the polarization direction of the linearly polarized light. The discrete asterisks represent the experimentally measured intensities of the reflected light at 640 nm from samples 1, 2, 3 and 4, respectively. Since the experimental results agree very well with the predicted values, it unambiguously shows that the four metasurfaces can rotate the *y*-polarized incident light to the designed angles. As the geometric phase does not depend on the wavelengths of the incident light, the metasurface devices are expected have broadband performance. Unsurprisingly, the good agreement between experimental values and simulation results is also found for the wavelengths of 550 nm, 800 nm and 1000 nm, which are shown in Figs. 4(a)-(c).

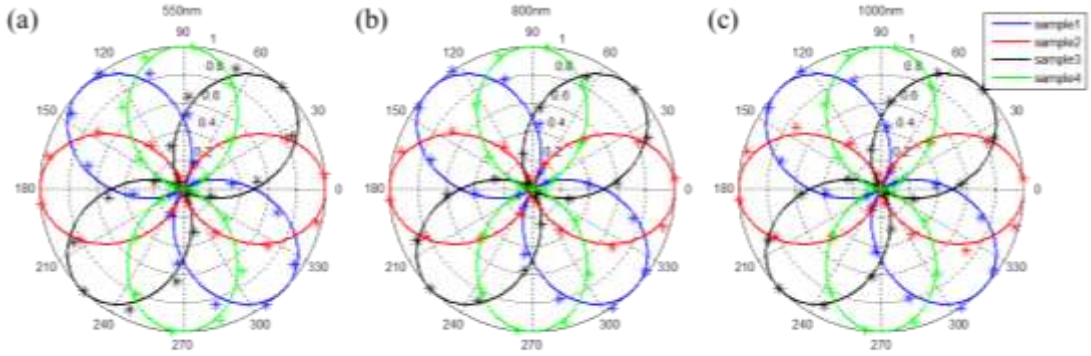

FIG. 4. Broadband performance of the metasurface for polarization rotation. The experimental results are obtained at the wavelengths of (a) 550nm, (b) 800nm and (c) 1000nm.

Only the $\pm1^{st}$, $\pm2^{nd}$ …and higher orders are the beams with rotated polarization direction, hence the efficiency should be calculated as the total power of the polarization-rotated light divided by the power of the incident light. Since the power for $\pm2^{nd}$ and higher diffraction orders is much lower than that of the $\pm1^{st}$ orders based on our measurement, only the $\pm1^{st}$ orders are take into consideration

when calculating the efficiency. Sample 4 is experimentally tested and its efficiency is measured to be 21.7%, 44.7% and 45.6% for the wavelengths of 640 nm, 800 nm and 1000 nm, respectively. The metasurface parameters in this paper, such as the nanorod size and the SiO_2 spacer thickness are the same with our previous design [28]. However, the conversion efficiency is slightly different due to the fabrication errors. The dielectric interlayer (SiO_2) sandwiched between the silver nanorods on the top and the silver layer at the bottom helps to eliminate the dispersion of the reflected light, leading to the broadband performance. Although the plasma frequencies of the silver lie in the ultraviolet region of the spectrum, the interband transition exerts a huge influence on its properties in the visible range. Hence silver is a good candidate for visible and near infrared light, but not for ultraviolet light due to the strong absorption. This bandwidth is closely related to the configuration parameters including the thickness of the spacer, rod size and packing density of the nanorods.

The reflective metasurface can reach the maximum conversion efficiency when the incident light is at normal incidence, any deviation from this case will lower the efficiency [28]. However, the polarization rotation functionality still exists for the tilted incident light at a certain scope (the metasurface works well for the 15.2° incident light according to our experiment).

Despite the fact that the device can operate in the broadband from the point of view of the conversion efficiency and polarization rotation functionality, it is worth noting that the reflection angle of the n^{th} order is governed by $\psi_n = \arctan(\lambda n/d)$, meaning that it depends on the incident wavelength. Since the nanorods are uniformly distributed in the *y*-direction as shown in Fig. 1(b), there will be no higher diffraction orders deviating from the designed plane of reflection (*xz* plane) for the wavelengths even shorter than double distance of neighboring distance *d*. It is worth noting that the polarization rotation of the reflected light by metasurfaces has some formal resemblance with the magneto-optical Kerr effect [31], where the polarization direction of the reflected light from a magnetic film is rotated as well. This effect is attributed to the antisymmetric, off-diagonal elements in the dielectric tensor of the magnetic film. In contrast, the polarization rotation realized here is through the collective contribution from all the nanorods in the inhomogeneous metasurface.

Conclusions

In conclusion, we propose and experimentally demonstrate an approach capable of rotating the polarization plane of the linearly polarized light in the visible and near infrared spectrum. Optical rotation is realized through the collective contribution of all the nanorods in the metasurface, instead of a single nanoantenna. In comparison with previously demonstrated approaches, our method proposed here can realize arbitrary polarization rotation angles with great fabrication tolerances and broadband performance. As this

approach solves several major issues typically associated with optical rotation: volume, efficiency and simplicity, it paves the way for future practical devices with optical rotation functionalities that may lead to advances in device miniaturization and system integration.

Acknowledgements. Engineering and Physical Sciences Research Council of the United Kingdom (Grant Ref: EP/M003175/1) and EPSRC IAA grant. China Scholarship Council (CSC, No. 201608310007 and 201606200099).

References

[1] L. D. Barron, *Molecular light scattering and optical activity*, Cambridge University Press, Cambridge, UK (2004**)**.

[2] A. I. Rusanov, and A. G. Nekrasov, Langmuir **26**, 13767 (2010).

[3] Y. A. He, B. Wang, R. K. Dukor, and L. A. Nafie, Appl. Spectrosc. **65**, 699 (2011).

[4] H. J. Rhee, Y. G. June, J. S. Lee, K. K. Lee, J. H. Ha, Z. H. Kim, S. J. Jeon, and M. H. Cho, Nature **458**, 310 (2009).

[5] D. Floess, J. Y. Chin, A. Kawatani, D. Dregely, H. U. Habermeier, T. Weiss, and H. Giessen, Light-Sci. Appl. **4**, e284 (2015).

[6] J. Y. Chin, T. Steinle, T. Wehlus, D. Dregely, T. Weiss, V. I. Belotelov, B. Stritzker, and H. Giessen, Nat. Commun. **4**, 1599 (2013).

[7] J. K. Gansel, M. Thiel, M. S. Rill, M. Decker, K. Bade, V. Saile, G. von Freymann, S. Linden, and M. Wegener, Science **325**, 1513 (2009).

[8] S. Zhang, Y.-S. Park, J. Li, X. Lu, W. Zhang, and X. Zhang, Phys. Rev. Lett. **102**, 023901 (2009).

[9] D.-H. Kwon, D. H. Werner, A. V. Kildishev, and V. M. Shalaev, Opt. Express **16**, 11822 (2008).

[10] E. Plum, J. Zhou, J. Dong, V. A. Fedotov, T. Koschny, C. M. Soukoulis, and N. I. Zheludev, Phys. Rev. B **79**, 035407 (2009).

[11] N. Yu, P. Genevet, M. A. Kats, F. Aieta, J.-P. Tetienne, F. Capasso, and Z. Gaburro, Science **334**, 333 (2011).

[12] A. V. Kildishev, A. Boltasseva, and V. M. Shalaev, Science **339**, 1232009 (2013).

[13] N. K. Grady, J. E. Heyes, D. R. Chowdhury, Y. Zeng, M. T. Reiten, A. K. Azad, A. J. Taylor, D. A. R. Dalvit, and H.-T. Chen, Science **340**, 1304 (2013).

[14] D. Wen, F. Yue, S. Kumar, Y. Ma, M. Chen, X. M. Ren, P. E. Kremer, B. D. Gerardot, M. R. Taghizadeh, G. S. Buller, and X. Z. Chen, Opt. Express **23**, 10272 (2015).

[15] F. Yue, D. Wen, J. Xin, B. D. Gerardot, J. Li, and X. Chen, Acs Photonics **3**, 1558 (2016).

[16] A. Papakostas, A. Potts, D. M. Bagnall, S. L. Prosvirnin, H. J. Coles, and N. I. Zheludev, Phys. Rev. Lett. **90**, 107404 (2003**)**.

[17] M. Kuwata-Gonokami, N. Saito, Y. Ino, M. Kauranen, K. Jefimovs, T. Vallius, J. Turunen, and Y. Svirko, Phys. Rev. Lett. **95**, 227401 (2005).

[18] F. Ding, Z. Wang, S. He, V. M. Shalaev, and A. V. Kildishev, ACS NANO **9**, 4111 (2015**)**.

[19] A. Pors, M. G. Nielsen, and S. I. Bozhevolnyi, Opt. Lett. **38**, 513 (2013).

[20] Z. H. Jiang, L. Lin, D. Ma, S. Yun, D. H. Werner, Z. Liu, and T. S. Mayer, Sci. Rep. **4**, 7511 (2014**)**.

[21] A. Shaltout, J. Liu, V. M. Shalaev, and A. V. Kildishev, Nano Lett. **14**, 4426 (2014**)**.

[22] P. C. Wu, W. Y. Tsai, W. T. Chen, Y. W. Huang, T. Y. Chen, J. W. Chen, C. Y. Liao, C. H. Chu, G. Sun, and D. P. Tsai, Nano Lett. **17**, 445 (2017).

[23] D. Lin, P. Fan, E. Hasman, and M. L. Brongersma, Science **345**, 298 (2014**)**.

[24] A. Arbabi, Y. Horie, M. Bagheri, and A. Faraon, Nat. Nano. **10**, 937 (2015**)**.

[25] K. Bliokh, F. Rodríguez-Fortuño, F. Nori and A. Zayats, Nat. Photon. **9**, 796 (2015).

[26] G. Zheng, H. Mühlenbernd, M. Kenney, G. Li, T. Zentgraf, and S. Zhang, Nat. Nano. **10**, 308 (2015**)**.

[27] W. J. Luo, S. Y. Xiao, Q. He, S. L. Sun, and L. Zhou, Adv. Opt. Mater. **3**, 1102 (2015**)**.

[28] D. Wen, F. Yue, G. Li, G. Zheng, K. Chan, S. Chen, M. Chen, K. F. Li, P. W. H. Wong, K. W. Cheah, E. Yue Bun Pun, S. Zhang, and X. Chen, Nat. Commun. **6**, 8241 (2015**)**.

[29] J. Goodman, *Introduction to Fourier Optics*, The McGraw-Hill Companies, Inc., New York, USA (1996**)**.

[30] N. Lv, *Fourier Optics*, China Machine Press, Beijing, China (2006**)**.

[31] Z. Q. Qiu and S. D. Bader, Rev. Sci. Instrum. **71**, 1243 (2000).